Thermal stress cleaving of silicon wafer by pulsed Nd:YAG laser

Jian Liu (刘 剑)*, Jian Lu (陆 建), Xiaowu Ni (倪晓武), Gang Dai (戴 罡), and Liang Zhang (张 梁)

Department of Applied Physics, Nanjing University of Science & Technology, Nanjing 210094, China

**E-mail: liujiannjlg@yahoo.com.cn*

Received March 23, 2010

The applied laser energy absorbed in a local area in laser thermal stress cleaving of brittle materials using a controlled fracture technique produces tensile thermal stress that causes the material to separate along the moving direction of the laser beam. The material separation is similar to crack extension, but the fracture growth is controllable. Using heat transfer theory, we establish a three-dimensional (3D) mathematical thermoelastic calculational model containing a pre-existing crack for a two-point pulsed Nd:YAG laser cleaving silicon wafer. The temperature field and thermal stress field in the silicon wafer are obtained by using the finite element method (FEM). The distribution of the tensile stress and changes in stress intensity factor around the crack tip are analyzed during the pulse duration. Meanwhile, the mechanism of crack propagation is investigated by analyzing the development of the thermal stress field during the cleaving process.

OCIS codes: 140.0140, 140.3390.
doi: 10.3788/COL20100810.1000.

The conventional mechanical cutting technique for brittle materials, in which cutting is aided by a metal- or diamond-point tool, has been used for decades. However, chip formation and fractures on cut edges are intractable problems in the cutting process. Various laser-cutting techniques, such as laser scribing and evaporation and controlled fracture technique, have recently been used in the industry.

The controlled fracture technique exhibits tremendous potential in laser cutting of brittle materials. It uses less laser power and enables high cutting speed compared with other laser cutting methods[1]. This technique involves cutting below the melting temperature of the brittle material—a practice that results in smooth edges. The laser cutting of thick ceramic substrates through the controlled fracture technique was investigated[2]. Tsai *et al.*[3] divided the cutting process into three stages: in the first stage, fracture initiated because of tensile stress; in the second stage, stable crack growth was observed; in the third stage, the crack extended unstably because of complete domination of tensile stresses. Yan *et al.* investigated crack characteristics during laser processing[4]. Ma *et al.* designed two kinds of laser cutting methods for boron carbides and discussed the effect of technical parameters on cutting quality[5]. Jiao *et al.* proposed a dual-laser-beam method to cut glass substrates[6]. An off-focus CO_2 laser beam was used to preheat the glass sample to reduce the thermal gradients, and a focused CO_2 laser beam was used to machine the glass. Nisar *et al.*[7] examined the cut deviation problem by analyzing the stress fields in the glass during the laser cutting process. Yamada *et al.* used two kinds of effective methods to reduce the thermal damage of the cut edge: a cleaving with pulsed Nd:YAG laser, and the application of a refrigerating chuck for the cleaving using continuous wave (CW) laser[8]. Ueda *et al.* investigated the cleaving mechanism of a silicon wafer irradiated with pulsed Nd:YAG laser[9]. The experimental results showed that the temperature at the area irradiated with the laser is an important factor in controlling crack propagation and achieving low thermal damage.

Based on the controlled fracture technique, brittle materials can be separated by a two-point pulsed laser. The cutting mode differs from the common pulsed laser cutting mode, in which a laser scans along the cutting line (see Fig. 1). Figure 2 shows that the silicon wafer is separated by a two-point pulsed laser, and the separation surface induced by thermal stress is smooth.

The scanning paths of the two pulsed laser beams are located on both sides of the cutting line in the two-point pulsed Nd:YAG laser cutting mode. In this letter, the finite element method (FEM) is used to investigate the temperature field and thermal stress field during the cutting process. Meanwhile, the mechanism of crack propagation is investigated by analyzing the development of the changes in stress intensity factor during the pulse duration.

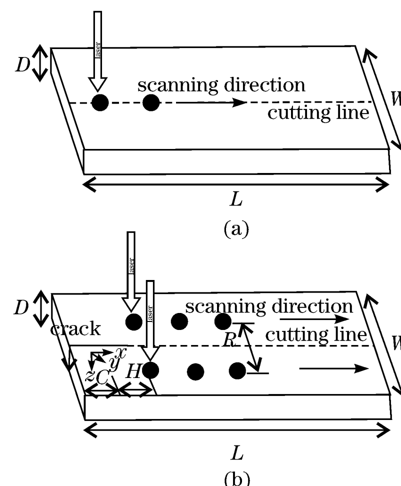

Fig. 1. Diagrams of the cutting process by (a) one-point pulsed laser and (b) two-point pulsed laser.

 © 2010 Chinese Optics Letters

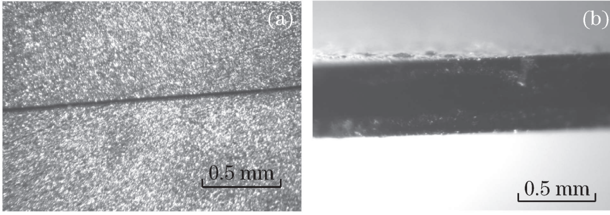

Fig. 2. Crack along cutting line induced by (a) thermal stress and (b) separation surface.

The dimension of the silicon wafer is 11.5 ×10 ×0.5 (mm). The wafer is irradiated by two moving pulsed laser beams and a pre-existing crack of 1.5-mm length is formed in the silicon wafer before cutting. This helps to initiate the crack and leads to the separation of the wafer. Figure 1(b) illustrates the laser cutting process.

Some assumptions are made before establishing the mathematical model as follows. 1) The physical parameters of the silicon are temperature-independent. 2) The superficial heat irradiation is negligible on the surface of the silicon wafer where there is no laser heating. 3) The cleaving direction and the crystal plane of the wafer are $<01\bar{1}>$ and $<100>$, respectively. 4) The specimen is annealed; thus, free of any residual stresses. 5) The stress-strain relationship of the silicon wafer is perfectly elastic.

Based on the assumptions above, the heat transfer model can be established as[10]

$$\rho c\frac{\partial T}{\partial t}=\kappa\left(\frac{\partial^2T}{\partial x^2}+\frac{\partial^2T}{\partial y^2}+\frac{\partial^2T}{\partial z^2}\right), \quad (1)$$

$$T(t)=T_0,\ \text{at}\ t=0, \quad (2)$$

$$-k\frac{\partial T}{\partial z}+h(T_\text{s}-T_0)=\varepsilon I(x,y,z,t),\ \text{at}\ z=0, \quad (3)$$

$$-k\frac{\partial T}{\partial n}=h(T_\text{n}-T_0),\ \text{at}\ z=-D,$$
$$x=0,\ \text{or}\ L, y=\pm\frac{W}{2}, \quad (4)$$

where k is the thermal conductivity, c and ρ are the heat capacity and density, respectively, T_0 denotes the initial temperature of the silicon (which is the same as the environment temperature); T_s and T_n denote the temperatures of the heated zone and area without laser heating, respectively; ε is the laser absorptivity; h represents the convection heat-transfer coefficient; $I(x,\ y,\ z,\ t)$ is the density of the laser power, n is the direction cosine of the boundary.

The laser beam maintains a constant TEM_{00} mode and travels in the x direction at constant velocity v. The density of the laser power can be described by Gaussian distribution as

$$I(x,y,t)=\frac{p_0}{\pi r^2}\exp\left(-\frac{x^2+y^2}{r^2}\right)g(t), \quad (5)$$

where $g(t)=\begin{cases}1, 0<t\le\tau\\ 0, t>\tau\end{cases}$, p_0, τ, and r are the power, the pulse duration, and the radius of the laser beam, respectively.

Stress and strain responses are assumed to be quasi-static at each interval, and the thermo-elastic model is used. During the laser cutting process, thermal stress may be induced by the thermal gradients in the silicon wafer, frequently caused by rapid heating or cooling. Thermal stress σ_therm caused by temperature difference ΔT is then derived by[11]

$$\sigma_\text{therm}=\frac{E\beta\Delta T}{1-\theta}, \quad (6)$$

where θ is the Poisson's ratio, and E and β are the Young's modulus and coefficient of linear expansion, respectively.

The FEM controlling equation for the temperature can be written as[12]

$$[\mathbf{K}]^\text{th}\{\mathbf{T}\}+[\mathbf{C}]\{\dot{\mathbf{T}}\}=\{\mathbf{Q}\}, \quad (7)$$

where $[\mathbf{K}]^\text{th}$, $[\mathbf{C}]$, $\{\mathbf{T}\}$, and $\{\dot{\mathbf{T}}\}$ are the heat conduction matrix, the heat capacity matrix, the temperature vector, and the temperature rise rate vector, respectively. The absorbed laser energy is expressed by heat source vector $\{\mathbf{Q}\}$. The Crank-Nicolson method[13] is used to solve Eq. (7). The temporal discrete form of Eq. (7) can be derived by

$$\left(\frac{1}{\Delta t}[\mathbf{C}]+\theta[\mathbf{K}]^\text{th}\right)\{\mathbf{T}\}_t=\left(\frac{1}{\Delta t}[\mathbf{C}]+(1-\theta)[\mathbf{K}]^\text{th}\right)$$
$$\{\mathbf{T}\}_{t+\Delta t}+\theta\{\mathbf{Q}\}_t+(1-\theta)\{\mathbf{Q}\}_{t+\Delta t}, \quad (8)$$

where Δt is the time interval and $\theta=1/2$.

The temperature increment is derived through $\Delta\text{T}=T_{t+\Delta t}-T_t$ as the temperature increases from T_t to $T_{t+\Delta t}$ during time interval Δt. The element strain induced by thermal expansion can be written in an incremental form in this manner[14]

$$\{\boldsymbol{\Delta}\varepsilon^\text{th}\}=\{\boldsymbol{\alpha}\}\Delta T, \quad (9)$$

where $\{\boldsymbol{\alpha}\}$ is the vector of thermal expansion coefficient. However, thermal expansion is restricted by the surrounding material, inducing thermal stress. The magnitude of thermal stress continues to grow in the elastic stage. Stress increment $\{\Delta\boldsymbol{\sigma}\}$ leads to elastic strain increment $\{\Delta\boldsymbol{\varepsilon}^\text{e}\}$. Total strain increment $\{\Delta\boldsymbol{\varepsilon}\}$ of the element can be expressed by[15]

$$\{\Delta\boldsymbol{\varepsilon}\}=\{\Delta\boldsymbol{\varepsilon}^\text{th}\}+\{\Delta\boldsymbol{\varepsilon}^\text{e}\}. \quad (10)$$

The stress-strain relationship in the elastic region is

$$\{\Delta\boldsymbol{\sigma}\}=\{\mathbf{D}\}^\text{e}(\{\Delta\boldsymbol{\varepsilon}\}-\{\Delta\boldsymbol{\varepsilon}^\text{th}\}-\{\Delta\boldsymbol{\varepsilon}_0\}), \quad (11)$$

where $\{\Delta\boldsymbol{\varepsilon}_0\}$ is introduced by elastic modulus E, and its expression is

$$\{\Delta\boldsymbol{\varepsilon}_0\}=\frac{\partial\left([\mathbf{D}]^\text{e}\right)^{-1}}{\partial T}\{\boldsymbol{\sigma}\}\,\text{d}T, \quad (12)$$

where $\{\mathbf{D}\}^\text{e}$ is the elastic matrix obtained by

$$[\mathbf{D}]^\text{e}=\frac{E}{(1+\mu)(1-2\mu)}\times\begin{bmatrix}1-\mu & \mu & \mu & 0\\ \mu & 1-\mu & \mu & 0\\ \mu & \mu & 1-\mu & 0\\ 0 & 0 & 0 & \frac{1-2\mu}{2}\end{bmatrix}, \quad (13)$$

Table 1. Physical Parameters of Silicon Wafer

ρ(kg·m^{-3})	C(J·k·g^{-1}·K^{-1})	k (W·m^{-1}·K^{-1})	β(K^{-1})	E(GPa)	σ	α(m^{-1})
2340	761	156	2.62×10^{-6}	117.4	0.262	5000

where μ is the Poisson's ratio. The incremental form of geometric equation on strain $\{\varepsilon\}$ and displacement $\{\mathbf{U}\}$ can be written as

$$\{\Delta\varepsilon\} = [\mathbf{B}]\{\Delta\mathbf{U}\}. \quad (14)$$

The equilibrium equation, which describes the relationship between displacement $\{\mathbf{U}\}$ and element thermal load vector $\{\mathbf{F}^{\text{th}}\}$, can also be written in incremental form[15]

$$[\mathbf{K}]\{\Delta\mathbf{U}\} = \{\Delta\mathbf{F}^{\text{th}}\}. \quad (15)$$

In the elastic region,

$$\left\{\Delta\mathbf{F}^{\text{th}}\right\} = \int_v [\mathbf{B}]^{\text{T}} [\mathbf{D}]^{\text{e}} \left(\left\{\Delta\varepsilon^{\text{th}}\right\} + \{\Delta\varepsilon_0\}\right) \text{d}V, \quad (16)$$

where $[\mathbf{B}]$ and $[\mathbf{K}]$ are the element geometric and element stiffness matrices, respectively.

The $[\mathbf{K}]$ and $\{\Delta\mathbf{F}^{\text{th}}\}$ of every element are assembled first. The incremental displacement of every node is then obtained by solving the total equilibrium equation. Furthermore, the strain increment $\Delta\varepsilon$ of every element is obtained by substituting the results into Eq. (14). Finally, the element stress increment is calculated by Eq. (11).

A finite element model is established based on FEM; the finite meshes of the model are shown in Fig. 3. A pre-existing crack is formed by setting two separate surfaces in the same location.

The pulsed Nd:YAG laser with the wavelength of 1.06 μm was used for cutting. The laser power, pulse duration, and beam radius are 567 W, 3 ms, and 0.9 mm, respectively. The one- and two-point laser cutting processes are simulated with this laser source to show the difference in the cleaving mechanism. The distance between the center of the first laser spot and the crack tip is 1.5 mm for the two-point laser cutting process, whereas the distance between the two laser spots is 3 mm. The material parameters are listed in Table 1[8].

Figure 4 shows the temperature curve of the central point of the laser spot. The temperature rapidly increases during laser irradiation. The maximum temperature of the center of the laser spot reaches 598 °C at 3 ms, which marks the end of irradiation. After the pulse duration, the temperature slowly descends as a result of heat loss by conduction.

Figure 5 shows the temperature distribution along the cutting line during the two-point pulsed laser cutting process. The temperature increases with the pulse duration. The temperature rises in the cutting line as a result of heat conduction because the temperature near the laser-heating zone in the scanning line is higher.

Figure 6 shows the temperature distribution along the cutting line at 3 ms in the two kinds of cutting modes. The pulsed laser moves along the cutting line in the one-

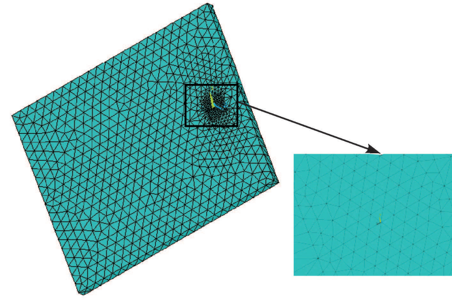

Fig. 3. Mesh of silicon wafer.

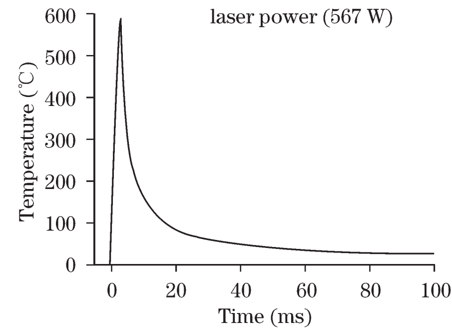

Fig. 4. Temperature curve of the central point of the laser spot.

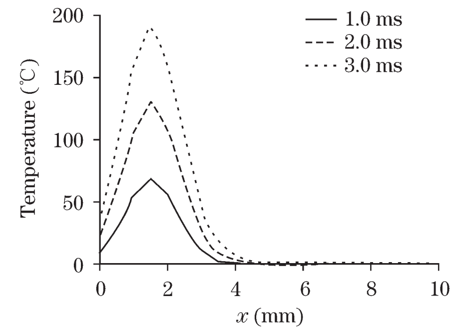

Fig. 5. Temperature distribution along the cutting line in the two-point laser mode.

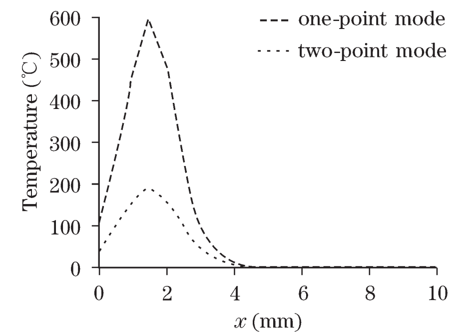

Fig. 6. Temperature distribution along the cutting line at 3 ms.

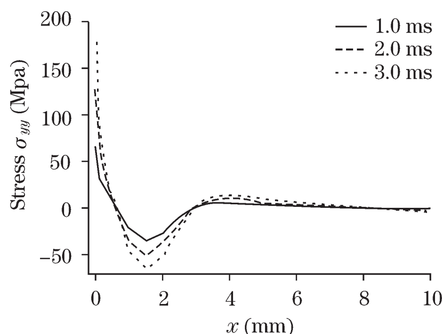

Fig. 7. Stress σ_{yy} distribution along the cutting line (two-point laser mode).

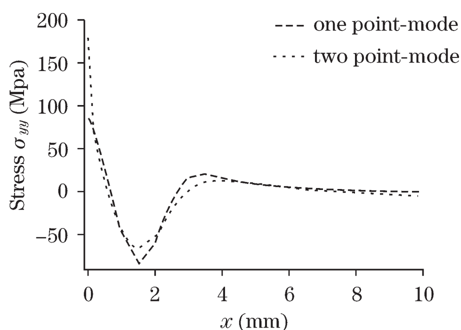

Fig. 8. Stress σ_{yy} distribution along the cutting line at 3 ms.

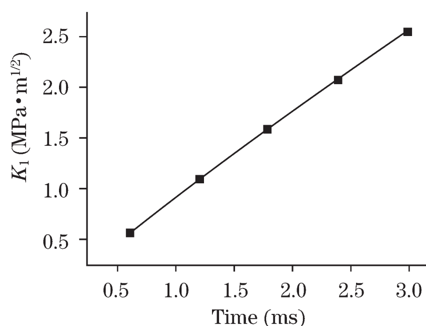

Fig. 9. Time curve of stress intensity K_1.

point laser cutting mode. The maximum temperature in the two-point laser cutting mode is lower than that in the one-point laser-cutting mode. The results of the simulation of the temperature field are consistent with the experimental results from the pulsed Nd:YAG laser processing silicon in Ref. [9].

Figure 7 shows normal stress σ_{yy} distribution along the cutting line during the two-point pulsed laser cutting process. The compressive stress is at its maximum at the point where the temperature is also the maximum at different times during the laser irradiation. The maximum tensile stress is always at the crack tip ($x = 0$) because of the stress concentration by the crack. The tensile stress at the crack tip constantly increases during the pulse duration. The crack propagates along the cutting line when the tensile stress induced by the laser becomes sufficiently high. The crack continues propagating by the end of the process when the maximum tensile stress in the next pulse duration is also at the new crack tip, caused by the stress concentration.

Figure 8 shows normal stress σ_{yy} distribution along the cutting line at 3 ms in the two kinds of cutting modes. The maximum compressive stress (85 MPa) induced by the laser heating in the one-point laser mode is higher than that (65 MPa) induced by heat conduction in the two-point laser cutting mode. The maximum tensile stress (182 MPa) in the two-point laser cutting mode is higher than that (90 MPa) in the one-point cutting mode.

The laser cutting process is the mode I fracture[16], and the crack propagates when stress intensity factor K_1 becomes larger than the fracture toughness of the material. Figure 9 shows the time history of stress intensity K_1 during the two-point laser cutting process. K_1 continues to increase during the laser irradiation time, when K_1 becomes higher than the fracture toughness (0.6 MPa·m$^{1/2}$of the silicon). The crack extension occurs at this point.

In conclusion, the temperature and thermal stress are calculated using FEM, based on the assumptions and the parameters of the silicon wafer, as well as the boundary conditions of the mathematical model. The tensile stress is produced at the crack tip and the stress intensity continues to increase during the laser irradiation time. The crack propagates when the stress intensity becomes higher than the fracture toughness of the material. The maximum tensile stress is always at the crack tip because of stress concentration in the entire cutting process. The simulation results in this letter agree with the experimental results in the pulsed Nd:YAG laser processing silicon in Refs. [7,8]. Cutting quality is improved if the parameters of the laser and the distance between the two laser spots are chosen properly; however, this area needs further investigation.

References

1. L. Ji, Y. Yan, Y. Bao, and Y. Jiang, Chinese J. Lasers (in Chinese) **35,** 1686 (2008).
2. C.-H. Tsai and H.-W. Chen, J. Mater. Process. Technol. **136,** 166 (2003).
3. C.-H. Tsai and C.-S. Liou, J. Manuf. Sci. Eng. **125,** 519 (2003).
4. Y. Yan, L. Ji, Y. Bao, and Y. Jiang, Chinese J. Lasers (in Chinese) **35,** 1401 (2008).
5. N. Ma, X. Wang, H. Ding, Y. Qian, S. Fu, and M. Hu, Chinese J. Lasers (in Chinese) **34,** 1441 (2007).
6. J. Jiao and X. Wang, Opt. Laser Technol. **40,** 297 (2008).
7. S. Nisar, M. A. Sheikh, L. Li, and S. Safdar, Opt. Laser Technol. **41,** 318 (2009).
8. K. Yamada, T. Ueda, A. Hosokawa, Y. Yamane, and K. Sekiya, Proc. SPIE **6107,** 61070H (2006).
9. T. Ueda, K. Yamada, K. Oiso, and A. Hosokawa, CIRP Annals-Manufacturing Technol. **51,** 149 (2002).
10. Z. H. Shen, S. Y. Zhang, J. Lu, and X. W. Ni, Opt. Laser Technol. **33,** 533 (2001).
11. D. Triantafyllidis, J. R. Bernstein, L. Li, and F. H. Stott, J. Laser Appl. **15,** 49 (2003).
12. S. Wu and Z. Ji, J. Mater. Process. Technol. **121,** 269 (2002).
13. J. Crank and P. Nicolson, Adv. Compute. Math. **6,** 207 (1996).
14. B. S. Yilbas, A. F. M. Arif, C. Karatas, and K. Raza, J. Mater. Process. Technol. **209,** 77 (2009).
15. Z. Liu, *Numerical Simulation of Heat Treatment Process* (in Chinese) (Science Press, Beijing, 1996).
16. J. Zhao, *Fracture Mechanics and Fracture Physics* (in Chinese) (Huazhong University of Science and Technology Press, Wuhan, 2003).